

An estimation of the local growth rate from Cosmicflows-3 peculiar velocities

Alexandra Dupuy¹ *, Helene M. Courtois¹, Bogna Kubik¹

¹University of Lyon, UCB Lyon 1, CNRS/IN2P3, IPN Lyon, 69622 Villeurbanne, France

20 March 2019

ABSTRACT

This article explores three usual estimators, noted as v_{12} of the pairwise velocity, ψ_1 and ψ_2 of the observed two-point galaxy peculiar velocity correlation functions. These estimators are tested on mock samples of *Cosmicflows-3* dataset (Tully et al. 2016), derived from a numerical cosmological simulation, and also on a number of constrained realizations of this dataset. Observational measurements errors and cosmic variance are taken into consideration in the study. The result is a local measurement of $f\sigma_8 = 0.43 (\pm 0.03)_{\text{obs}} (\pm 0.11)_{\text{cosmic}}$ out to $z = 0.05$, in support of a Λ CDM cosmology.

1 INTRODUCTION

Since the late 70's, several publications discussed the theory of galaxy pairwise peculiar velocity statistics, such as the 2-point peculiar velocity correlation function (ψ_1 and ψ_2) or the mean pairwise velocity (v_{12} ; Monin & Yaglom 1975; Davis & Peebles 1977; Peebles 1980, 1987; Gorski 1988). It has been shown that such statistics can be measured directly from only the radial part of peculiar velocities. Since these statistics are related to the growth factor of large scale structures $f = \Omega_m^\gamma$, where γ is the growth index (Lahav et al. 1991), observed peculiar velocities can be used as cosmological probes to estimate the matter density parameter Ω_m (Ferreira et al. 1999; Juszkiewicz et al. 1999). However, f and σ_8 , the amplitude of the density fluctuations on 8 Mpc h^{-1} scales (where $h = H_0/100$ and H_0 is the Hubble constant), are degenerate and cannot be constrained separately when using only galaxy peculiar velocity data.

The first attempts of constraining cosmological parameters such as the density parameter have been made by Peebles (1976), Kaiser (1990) and Hudson (1994). Later, Juszkiewicz et al. (2000) gave $\Omega_m = 0.35 \pm 0.15$ with measurements of the mean pairwise velocity on the *Mark III* catalog of radial peculiar velocities of roughly 3,000 spiral and elliptical galaxies (Willick et al. 1995, 1996, 1997). Then, Feldman et al. (2003) obtained a very similar value of $\Omega_m = 0.30^{+0.17}_{-0.07}$ and also measured $\sigma_8 = 1.13^{+0.22}_{-0.23}$. This was done by using the same estimator of Juszkiewicz et al. (2000), but on a much larger dataset combining peculiar velocities of approximately 6,400 galaxies extracted from several catalogs: *Mark III*, *Spiral Field I-Band* (Giovannelli et al. 1994, 1997a,b; Haynes et al. 1999a,b), *Nearby Early-type Galaxies Survey* (da Costa et al. 2000) and the *Revised Flat Galaxy Catalog* (Karachentsev et al. 2000).

A decade later, datasets improved and methods of analyzing peculiar velocity to constrain cosmology evolved. Some authors proposed new statistical methodologies using observed peculiar velocities, which differs from v_{12} and $\psi_{1,2}$,

in order to constrain the growth rate of large scale structures and related parameters. On the one hand, Hudson & Turnbull (2012) measured $f\sigma_8 \equiv \Omega_m^{0.55}\sigma_8 = 0.40 \pm 0.07$ by comparing the observed peculiar velocities of 245 supernovae (extracted from a compilation dubbed the *First Amendment*, A1) to the galaxy density field predicted by the *Point Source Catalogue Redshift Survey* (PSCz, Saunders et al. 2000). This method has been later applied by Carrick et al. (2015) on galaxies from the 2M++ redshift compilation (Lavaux & Hudson 2011), finding a much more accurate estimate of the growth factor $f\sigma_8 = 0.401 \pm 0.024$. On the other hand, Johnson et al. (2014) analyzed the two-point statistics of the peculiar velocity field and obtained $f\sigma_8 = 0.418 \pm 0.065$ from a sample gathering peculiar velocities of $\sim 9,200$ galaxies from the *Six Degree Field Galaxy Survey* peculiar velocity catalog (6dFGS, Jones et al. 2004, 2006, 2009) and various supernovae distance measurements. Alternatively, using again the same two-point statistic (v_{12}) as Juszkiewicz et al. (2000) and Feldman et al. (2003), applied on the *Cosmicflows-2* catalog containing $\sim 8,000$ galaxy distances (CF2, Tully et al. 2013), Ma et al. (2015) found surprising results: $\Omega_m^{0.6}h = 0.102^{+0.384}_{-0.044}$ and $\sigma_8 = 0.39^{+0.73}_{-0.1}$. Moreover, by measuring the covariance of radial peculiar velocities in two catalogs, a sample of 208 low redshift supernovae (named *SuperCal*) and a set of roughly 9,000 peculiar velocities from 6dFGS, Huterer et al. (2016) evaluated $f\sigma_8 = 0.428^{+0.048}_{-0.045}$ at $z = 0.02$. Finally, Adams & Blake (2017) measured $f\sigma_8 = 0.424^{+0.067}_{-0.064}$ by modelling the cross-covariance of the galaxy overdensity and peculiar velocity fields and applying their analysis to the observed peculiar velocities from the 6dFGS data.

Despite the increase in number of measurements and in redshift coverage, peculiar velocity catalogs are still not large enough and remain noticeably sparse at large distances. Hence, growth rate estimations are affected by uncertainties introduced by cosmic variance as they are obtained from local observations. Hellwing et al. (2016) discussed the effect

arXiv:1901.03530v2 [astro-ph.CO] 19 Mar 2019

of the observer location in the universe on the derivation of two-point peculiar velocity statistics (v_{12} , ψ_1 and ψ_2) by considering two sets of randomly chosen observers and Local Group-like observers. The authors showed that the local environment, especially the Virgo cluster, systematically introduces deviations from predictions.

More recently, Nusser (2017) measured $f\sigma_8 = 0.40 \pm 0.08$ by measuring velocity - density correlations on the largest and most recent catalog of $\sim 18,000$ accurate galaxy distances, *Cosmicflows-3* (CF3, Tully et al. 2016). And, last but not least, Wang et al. (2018) analyzed the peculiar velocity correlation functions through the estimators ψ_1 and ψ_2 applied to the *Cosmicflows* catalogs (CF2 and CF3) to constrain cosmological parameters: $\Omega_m = 0.315^{+0.205}_{-0.135}$ and $\sigma_8 = 0.92^{+0.440}_{-0.295}$.

On the grounds of the previous literature works introduced above, this article studies two classical two-point peculiar velocity statistics, using radial peculiar velocities provided by the *Cosmicflows-3* catalog, to constrain the local value of the growth rate factor $f\sigma_8$. Its structure is organized as follows. Section 2 provides details on the peculiar velocity data used for the analysis. The methodology of two-point correlation functions of peculiar velocities is described in Section 3 and is tested and validated on mocks in Section 4. Section 5 shows the velocity statistics measured on observed peculiar velocities. The main result of this article, the estimate of the growth rate from *Cosmicflows* radial peculiar velocities, is discussed in Section 6.

2 DATA

2.1 Observed peculiar velocities: *Cosmicflows-3*

The latest CF3 catalog (Tully et al. 2016) provides distances for 17,648 galaxies which can be redistributed within 11,936 groups, up to 150 Mpc h^{-1} . It is an expansion of the previous CF2 catalog (Tully et al. 2013). It contains 8,188 galaxy distances with a homogeneous volume coverage up to 80 Mpc h^{-1} , mostly derived with the Tully-Fisher (TF) relation (Tully & Fisher 1977), linking the luminosity to the HI line width for spiral galaxies, and the Fundamental Plane (FP) relation (Djorgovski & Davis 1987; Dressler 1987) for elliptical galaxies. The main additions to the CF3 catalog are new distances, obtained with the FP relation from 6dFGS, and distances computed with the TF relation. About 60 percent of CF3 distances are therefore measured with the FP method and mostly located in the Southern celestial hemisphere, while around 40 percent of distances are obtained with the TF relation. Few distance measurements are obtained from various methods where applicable such as Cepheids, Tip of the Red Giant Branch, type Ia Supernovae, and surface brightness fluctuations.

From the distance d of a galaxy and its redshift z , it is possible to derive the radial component of its peculiar velocity, $u = cz - H_0d$, where c is the speed of light in vacuum, and H_0 is the Hubble constant. However, as distance moduli have Gaussian distributed errors, the peculiar velocities computed with this equation have non-Gaussian (skewed) distributed errors. To solve this problem, Watkins & Feldman (2015) introduced a new estimator which results

in Gaussian distributed errors on peculiar velocities:

$$u = cz \ln \left(\frac{cz}{H_0d} \right). \quad (1)$$

Equation 1 will be used throughout this paper to derive radial peculiar velocities from observed distances.

This article will only focus on the CF3 distances catalog. Two radial peculiar velocity samples will be considered: the ungrouped sample and the grouped sample, containing galaxies and groups of galaxies respectively. Groups are frequently used by authors because they allow to reduce uncertainties with an \sqrt{N} improvement on observed distances, and thus on radial peculiar velocities. These uncertainties are due to the virial motions of group members. However, the methodology presented in this article is valid for pairs of galaxies, and not for pairs of groups of galaxies. The CF3 grouped catalog is tested in this article since recent studies (Ma et al. 2015; Nusser 2017, both introduced above in Section 1) made use of the grouped versions of the *Cosmicflows* catalogs to derive $f\sigma_8$. However, it will be seen in the discussion that using grouped data to constrain the growth rate leads to incoherent results.

Tully et al. (2016) shows that the most consistent value of the Hubble constant with CF3 distances when computing radial peculiar velocities is $H_0 = 75 \pm 2$ km s $^{-1}$ Mpc $^{-1}$. This value is preferred as it minimizes the monopole term with CF3 distances and results in a tiny global radial infall and outflow in the peculiar velocity field. A larger value of H_0 would give a large overall radial infall towards the position of the observer, while choosing a smaller H_0 would yield a large radial outflow (cf. Figure 21 in Tully et al. 2016).

For these reasons, in this article the value $H_0 = 75$ km s $^{-1}$ Mpc $^{-1}$ is used to compute radial peculiar velocities of CF3 galaxies and groups. We note that this high value of H_0 is consistent with other values of the Hubble constant measured in the local universe.

2.2 *Cosmicflows* mock catalogs

A three-dimensional peculiar velocity field computed with the Constrained Realization (CR) methodology (Hoffman & Ribak 1991) is considered to construct mock catalogs. Using the CF3 grouped dataset and assuming a Λ CDM cosmological model ($\Omega_m = 0.3$, dark energy density parameter $\Omega_\Lambda = 0.7$ and $H_0 = 70$ km s $^{-1}$ Mpc $^{-1}$), this velocity field is composed of a velocity field obtained with the Wiener-Filter technique (Zaroubi et al. 1995, 1999, WF) and a random component derived from the Random Realizations method. The velocity field used in this article is reconstructed in a box 2000 Mpc wide, in Cartesian Supergalactic coordinates and centered on the Milky Way, with 128^3 cells.

In order to test the various estimators of the peculiar velocity correlation function, mock catalogs are prepared as explained hereafter. Radial peculiar velocities, predicted by the three-dimensional velocity field of a CR, are assigned to galaxies or groups from the CF3 data. The mock catalogs are prepared with the following method. Considering galaxies and groups of the CF3 catalog, their predicted three-dimensional peculiar velocities are extracted from the CRs' peculiar velocity field at the redshift positions of the galaxies. The radial part of the peculiar velocity, which is the

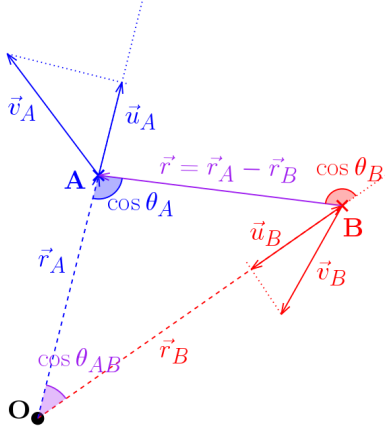


Figure 1. Pair of galaxies considered throughout this article.

only observable component, is then derived from the three-dimensional velocity.

Throughout this article, parameters that are not fixed by the cosmology of the CR are set to their Planck 2015 values (Planck Collaboration et al. 2016, $\Omega_\Lambda = 0.69$, $\Omega_m = 0.31$, $\sigma_8 = 0.82$).

3 METHODOLOGY

We consider in this article a pair of galaxies A and B located at the positions \vec{r}_A and \vec{r}_B respectively. The spatial separation of these two galaxies is given by $\vec{r} = \vec{r}_A - \vec{r}_B$. Their peculiar velocities are \vec{v}_A and \vec{v}_B and their radial components are given by $\vec{u}_A = u_A \hat{r}_A = (\vec{v}_A \cdot \hat{r}_A) \hat{r}_A$ and $\vec{u}_B = u_B \hat{r}_B = (\vec{v}_B \cdot \hat{r}_B) \hat{r}_B$, where $\hat{r}_{A,B}$ are the unit direction vectors of the galaxies. The cosines of the angles between the different directions are given by $\cos \theta_A = \hat{r}_A \cdot \hat{r}$, $\cos \theta_B = \hat{r}_B \cdot \hat{r}$ and $\cos \theta_{AB} = \hat{r}_A \cdot \hat{r}_B$. Figure 1 illustrates the geometry and quantities defined above.

To partially avoid the Malmquist bias, the galaxies (or groups) are located at their redshift positions, as positioning objects at their observed distance leads to much larger errors, especially for the most distant ones.

3.1 Mean pairwise velocity

3.1.1 Model

The mean pairwise velocity v_{12} was introduced for the first time in the context of the Bogolyubov-Born-Green-Kirkwood-Yvon theory (BBGKY, Yvon 1935; N. N. Bogolyubov 1946; Kirkwood 1946, 1947; Born & Green 1946). In this theory, the conservation equation of pairs of galaxies links the two-point correlation function $\xi(r)$ to the growth rate of large scale structures f and the mean pairwise velocity $v_{12}\vec{r}/r$ (Davis & Peebles 1977; Peebles 1980). For a pair of galaxies separated by a distance r , the mean pairwise velocity is given by (Juszkiewicz et al. 1998):

$$v_{12}(r) = \left\langle (\vec{u}_A - \vec{u}_B) \cdot \hat{r} \right\rangle_\rho = \frac{\langle (\vec{u}_A - \vec{u}_B) \cdot (1 + \delta_A)(1 + \delta_B) \rangle}{1 + \xi(r)}, \quad (2)$$

where \vec{u}_i and δ_i correspond respectively to the peculiar velocity and the density contrast at the location of the galaxies $i = A, B$, and $\langle \dots \rangle_\rho$ specifies a pair-weighted average with $(1 + \delta_A)(1 + \delta_B)(1 + \xi(r))^{-1}$ as the weighting factor.

In the non-linear regime, i.e for pairs of very close galaxies, $\xi(r) \gg 1$, and the solution of the pair conservation equation is $v_{12}(r) = -H_0 r$. In the case of the linear regime, i.e for large separation distances, $\xi(r) \ll 1$ and the solution of the conservation equation for v_{12} is then given by the perturbative expansion of $\xi(r)$. In order to measure cosmological parameters such as the total matter density parameter Ω_m , Juszkiewicz et al. (1999) introduce a solution for v_{12} valid in both regimes, linear and non-linear, by interpolating the linear and non-linear solutions:

$$v_{12}(r) \approx -\frac{2}{3} H r f \bar{\xi}(r) \left[1 + \alpha \bar{\xi}(r) \right], \quad (3)$$

where $\bar{\xi}(r) = \bar{\xi}(r)/[1 + \xi(r)]$ and $\bar{\xi}(r) = 3r^{-3} \int_0^r \xi(x)x^2 dx$ is the two-point correlation function averaged in a sphere of radius r . The parameter $\alpha = 1.2 - 0.65\gamma$ depends on the logarithmic slope of $\xi(r)$ denoted by the quantity $0 < \gamma < 3$ given by:

$$\gamma = - \left. \frac{d \ln \xi(r)}{d \ln r} \right|_{\xi=1}. \quad (4)$$

From the approximate solution for v_{12} (equation 3), it is possible to recover the linear solution if $\xi \rightarrow 0$, and the solution valid in the non-linear regime if $x \rightarrow 0$. Equation 3 has been tested and validated by Juszkiewicz et al. (1999) on N-body simulations for $0.1 < \xi(r) < 1000$.

3.1.2 Estimator

Equation 3 shows that the amplitude of the mean pairwise velocity v_{12} is related to the growth rate f , as shown in the left panel of Figure 2. The statistic v_{12} can therefore be used to constrain this parameter. However, observations give access only to the radial part of the peculiar velocities of galaxies. Therefore, one cannot use equation 3 to compute v_{12} directly from observed data. An estimator that can be used to compute $v_{12}(r)$ directly from observed radial peculiar velocities has to be considered. Ferreira et al. (1999) introduced such an estimator to determine the mean pairwise velocity directly for observational catalogs of peculiar velocities:

$$v_{12}(r) = \frac{2 \sum (u_A - u_B)(\cos \theta_A + \cos \theta_B)}{\sum (\cos \theta_A + \cos \theta_B)^2}, \quad (5)$$

where the sums are computed for all pairs separated by a distance r .

A new estimator which relies on the transverse component of peculiar velocities (instead of the radial one) has been introduced by Yasini et al. (2018). This estimator will allow to analyze pairwise velocities derived from upcoming transverse peculiar velocity surveys such as Gaia (Hall 2018).

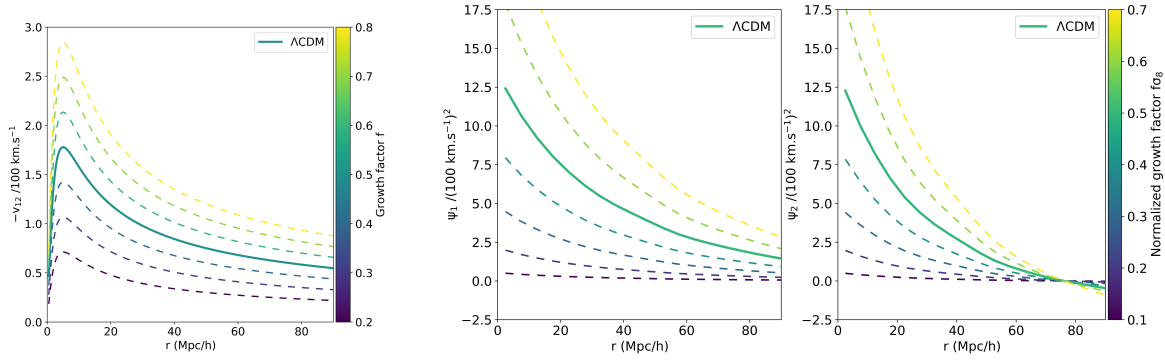


Figure 2. Λ CDM models of the three usual peculiar velocity statistics v_{12} (left), ψ_1 (middle) and ψ_2 (right) as a function of the pair separation r . The three statistics are computed for several values of $f\sigma_8$ (see colorbar).

3.2 Velocity correlation function

In the linear regime, the two-point correlation tensor of a homogeneous and random velocity field $\vec{v}(\vec{r})$ is defined as (Monin & Yaglom 1975; Strauss & Willick 1995):

$$\Psi_{ij}(r) \equiv \langle v_i(\vec{r}_A)v_j(\vec{r}_B) \rangle = [\Psi_{\parallel}(r) - \Psi_{\perp}(r)] \hat{r}_i \hat{r}_j + \Psi_{\perp}(r) \delta_{ij}, \quad (6)$$

where i and j are the Cartesian coordinates. The quantities $\Psi_{\parallel}(r)$ and $\Psi_{\perp}(r)$ are the radial (i.e. along \vec{r}) and transverse velocity correlation functions respectively. The spectral representations of $\Psi_{\parallel}(r)$ and $\Psi_{\perp}(r)$ are given by (Gorski 1988):

$$\Psi_{\parallel}(r) = \frac{H_0^2 (f\sigma_8)^2}{2\pi^2} \int P_0(k) \left[j_0(kr) - 2 \frac{j_1(kr)}{kr} \right] dk \quad (7)$$

and

$$\Psi_{\perp}(r) = \frac{H_0^2 (f\sigma_8)^2}{2\pi^2} \int P_0(k) \frac{j_1(kr)}{kr} dk \quad (8)$$

where $j_0(x)$ and $j_1(x)$ are the spherical Bessel functions of the first kind:

$$j_0(x) = \frac{\sin x}{x}, \quad j_1(x) = \frac{\sin x}{x^2} - \frac{\cos x}{x}, \quad (9)$$

and $P_0(k)$ is the non-normalized linear matter power spectrum measured today. In the rest of this article $P_0(k)$ is computed with CAMB in the Planck 2015 cosmology.

The quantities $\Psi_{\parallel}(r)$ and $\Psi_{\perp}(r)$ both depend on the parameter $(f\sigma_8)^2$. These correlation functions can therefore be used to constraint the combined cosmological parameter $f\sigma_8$, defined as the normalized growth rate of large scale structures.

3.2.1 Estimator

Gorski et al. (1989) introduced two velocity statistics, noted here as ψ_1 and ψ_2 , which depend only on radial peculiar velocities. The statistic ψ_1 is defined as:

$$\psi_1(r) = \frac{\sum \vec{u}_A \cdot \vec{u}_B}{\sum (\hat{\vec{r}}_A \cdot \hat{\vec{r}}_B)^2} = \frac{\sum u_A u_B \cos \theta_{AB}}{\sum \cos^2 \theta_{AB}}, \quad (10)$$

and ψ_2 as:

$$\psi_2(r) = \frac{\sum (\vec{u}_A \cdot \hat{\vec{r}}) (\vec{u}_B \cdot \hat{\vec{r}})}{\sum (\hat{\vec{r}}_A \cdot \hat{\vec{r}}_B) (\hat{\vec{r}}_A \cdot \hat{\vec{r}}) (\hat{\vec{r}}_B \cdot \hat{\vec{r}})} = \frac{\sum u_A u_B \cos \theta_A \cos \theta_B}{\sum \cos \theta_{AB} \cos \theta_A \cos \theta_B}, \quad (11)$$

The sums in equations 10 and 11 are performed over all pairs with fixed separation r . The denominators normalize the sums in order to preserve the norm of the velocity field.

3.2.2 Model

The correlation function of radial peculiar velocities can be derived from the two-point velocity correlation tensor:

$$\langle u_m(\vec{r}_A) u_n(\vec{r}_B) \rangle = \hat{r}_{Am} \hat{r}_{Bn} \Psi_{ij}(r) \hat{r}_{Ai} \hat{r}_{Bj}, \quad (12)$$

where i, j, m and n are the Cartesian coordinates. Inserting equation 12 into equations 10 and 11, the quantities $\psi_1(r)$ and $\psi_2(r)$ can be written as functions of $\Psi_{\parallel}(r)$ and $\Psi_{\perp}(r)$ (Gorski et al. 1989):

$$\psi_{1,2}(r) = \mathcal{A}_{1,2}(r) \Psi_{\parallel}(r) + [1 - \mathcal{A}_{1,2}(r)] \Psi_{\perp}(r), \quad (13)$$

where

$$\mathcal{A}_1(r) = \frac{\sum \cos \theta_A \cos \theta_B \cos \theta_{AB}}{\sum \cos^2 \theta_{AB}}, \quad (14)$$

and

$$\mathcal{A}_2(r) = \frac{\sum \cos^2 \theta_A \cos^2 \theta_B}{\sum \cos \theta_A \cos \theta_B \cos \theta_{AB}}. \quad (15)$$

The functions $\mathcal{A}_1(r)$ and $\mathcal{A}_2(r)$ contain information about the geometry of the sample, and measure the contributions of $\Psi_{\parallel}(r)$ and $\Psi_{\perp}(r)$ to the functions $\psi_1(r)$ and $\psi_2(r)$.

As one can see on the middle and right panels of Figure 2, the amplitude of the two statistics ψ_1 and ψ_2 depends on the growth factor $f\sigma_8$, allowing to constrain this cosmological parameter. The higher $f\sigma_8$ is, the higher the amplitude of ψ_1 or ψ_2 is: a universe with a large $f\sigma_8$ appears more compact and peculiar velocities get larger. However, in the

case of ψ_2 , the curves corresponding to different $f\sigma_8$ get closer and closer as r increases (see right panel of Figure 2). It is difficult to constrain cosmological models for separation distances higher than 60 Mpc/ h . The statistic ψ_2 is therefore not robust enough to estimate the growth rate on peculiar velocity catalogs such as CF3, and especially on the upcoming big surveys. Therefore, this statistic will not be considered for the rest of this paper.

3.3 Observational errors and cosmic variance

Two kinds of uncertainties on peculiar velocity statistics are considered in this article: measurement (or observational) error and cosmic variance.

Observational errors on peculiar velocity statistics v_{12} , ψ_1 and ψ_2 , i.e errors due to the uncertainty in distance measurement, are derived by Monte-Carlo synthetic realizations. These realizations are constructed by adding a random error to the radial peculiar velocity. The random error is extracted from a normal distribution with a standard deviation equal to the measurement error on the peculiar velocity. This measurement error is derived from the uncertainty on the distance (or distance modulus). In this article, 100 realizations have been computed for each sample (mocks and observed data).

In addition to measurements uncertainties, one ought to take into account the impact of cosmic variance when estimating cosmological parameters. However, computing uncertainties caused by cosmic variance cannot be done on a Constrained Realization of CF3, described in section 2, which represents our local universe. Therefore, a Λ CDM dark matter only N -body simulation is considered in this paper in order to estimate the impact of the cosmic variance on peculiar velocity statistics and growth rate measurements. Two tests, whose results are presented later in this paper, on dark matter halos extracted from the MultiDark Planck 2 simulation (MDPL2, Prada et al. 2012) of size 1 Gpc h^{-1} are carried out. The underlying cosmology of the simulation is the Planck 2015 cosmology. Only mock galaxies with halo mass between $10^{11} M_\odot$ and $10^{12} M_\odot$ are taken into account to construct these mocks. Data samples for the tests are prepared as follows:

- as the CF3 catalog can (mostly) be contained in a sphere of a 250 Mpc h^{-1} radius, one can place 8 of such independent spheres in a cube of side 1 Gpc h^{-1} . Therefore 8 CF3-like samples are generated for each octant cube of the simulation. The observer of each sample is placed at the center of its associated octant. Then radial components of peculiar velocities are extracted at the position of CF3 galaxies with respect to the observer. These mocks are completely independent from each other as they do not share any halos.

- As only 8 samples is not high enough to get a robust result, a total of 100 more mocks are generated. Instead of positioning observers such that samples do not share halos, a total of 100 observers are placed at a random locations within the simulation box. Then radial components of peculiar velocities are extracted at the position of CF3 galaxies with respect to the observers. In this case, the samples are not independent as a single halo can belong to several spheres, so results will be correlated.

Results obtained from these tests are shown in section 4.

As different bins of separation distances share the same galaxies (or groups of galaxies), errors between bins are correlated and thus the covariance matrix needs to be considered when fitting the measured statistics to extract the normalized growth rate $f\sigma_8$.

From these Monte-Carlo realizations or cosmic variance mocks, the covariance matrix C between bins of separation distances of galaxy pairs can be computed. The covariance between bins r_m and r_n is computed as:

$$C_{mn} = \frac{1}{N_k - 1} \sum_{k=1}^{N_k} (S_k(r_m) - \overline{S_m}) (S_k(r_n) - \overline{S_n}) \quad (16)$$

where S denotes the statistic considered and $\overline{S_{m,n}} = \frac{1}{N_k} \sum_{k=1}^{N_k} S_k(r_{m,n})$ is defined as the mean of all realizations for the bins r_m and r_n respectively and $N_k = 100$ is the number of mocks (realizations).

4 DERIVING THE LOCAL GROWTH RATE

4.1 Verification of estimators on mocks

The normalized growth rate $f\sigma_8$ is estimated by fitting the theoretical models of the statistics v_{12} and ψ_1 , noted S_{mod} and computed with equation 3 and 13, to the quantity S_{meas} measured with the radial estimators of the two statistics defined in equations 5 and 10 respectively. The value of the growth rate $f\sigma_8$ is obtained by minimizing the following chi-square function:

$$\chi^2(f\sigma_8) = \sum_{i,j=0}^{N_{\text{bins}}} \left[(S_{\text{meas}}(r_i) - S_{\text{mod}}(r_i; f\sigma_8)) C_{ij}^{-1} (S_{\text{meas}}(r_j) - S_{\text{mod}}(r_j; f\sigma_8)) \right] \quad (17)$$

The minimization is conducted with MINUIT (Function Minimization and Error Analysis software, James & Roos 1975). The error on the fitted parameter is also given by MINUIT as the second derivative of the chi-square.

Peculiar velocity statistics v_{12} and ψ_1 have been measured on mock and observed radial peculiar velocities. Throughout this article, statistics are computed out to a distance of 100 Mpc h^{-1} in 20 equal bins of 5 Mpc h^{-1} . In all figures of this article displaying velocity statistics computed on mocks or observed data, scattered points are located at the middle of the bins.

The statistics v_{12} and ψ_1 have been tested and validated by the authors who introduced them. They allow one to recover the underlying cosmology from a homogeneous and spherical universe. But CF3 is very sparse and asymmetrical. Before constraining the growth rate, one must check if the spatial distribution of the CF3 catalog alone inhibits such statistics from accurately recovering the underlying cosmology. This is done on the 100 CF3 mocks generated from a Constrained Realization as described in section 2.

Figure 3 shows as solid lines the Λ CDM models for galaxies in the CF3 ungrouped (red) and CF3 grouped (blue) mocks. For the statistic v_{12} , errors bars of the two mocks do not include the Λ CDM model. This means that due to the

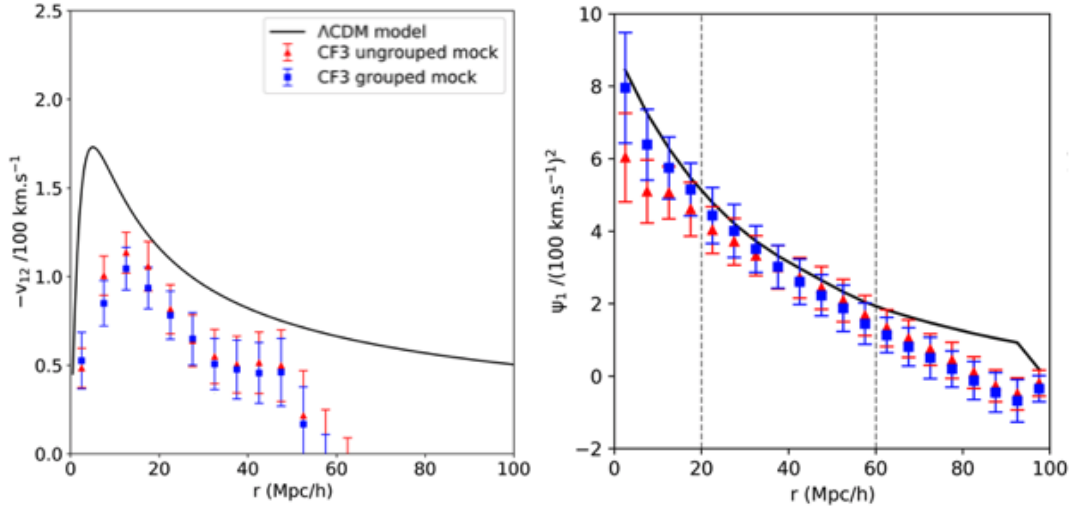


Figure 3. The two peculiar velocity statistics v_{12} (left) and ψ_1 (right) as a function of the pair separation r . The Λ CDM model ($\Omega_m = 0.3$, $\gamma = 0.55$, $\sigma_8 = 0.82$) is shown as a black solid line. Scattered points with error bars represent results obtained from mock peculiar velocities constructed from a Λ CDM constrained realization of CF3. The CF3 ungrouped and grouped mocks are shown as red triangles and blue squares respectively. Vertical dashed lines show the region where $f\sigma_8$ can be fitted, see the limitations described in the text.

unique CF3 geometry and selection function, this estimator can not recover the underlying Λ CDM cosmology. Therefore we stress that it cannot be used to estimate to local growth rate with the real CF3 catalog, and will not be considered in the analysis that follows. Also, this explains why [Ma et al. \(2015\)](#) obtained incoherent values for Ω_m and σ_8 by applying v_{12} on the CF2 dataset, whose footprint is similarly inhomogeneous. For the estimator ψ_1 , the amplitude of the CF3 mocks (red and blue dots with error bars for the ungrouped and grouped samples respectively) is slightly lower but error bars are consistent with the models up to $60 \text{ Mpc } h^{-1}$. This shows that the geometry and the sparseness of the current survey prevent from deriving any growth rate for separation distances larger than $60 \text{ Mpc } h^{-1}$.

Furthermore, one can see in [Figure 3](#) that for both statistics the overall differences between the CF3 grouped and ungrouped samples are very small. This shows that non-linearity does not have any impact on the ψ_1 estimator except for small separations bins which contain galaxies close to each other (i.e within clusters). When fitting $f\sigma_8$ to this statistic, the effect of non-linearity will not be taken into account: bins corresponding to separations lower than $20 \text{ Mpc } h^{-1}$ will be omitted.

Tests on mocks reported in [Figure 3](#) show that the underlying value of $f\sigma_8$ in the CR is recovered by the estimator ψ_1 in an interval of robustness $20 - 60 \text{ Mpc}/h$. However, considering the depth of the CF3 catalog and the size of the constrained realization, the measured value of the growth rate with CF3 datasets gives only its local value. Due to cosmic variance, this local value may not represent the global value of the growth rate of large scale structures of the entire universe.

[Figure 4](#) shows peculiar velocity statistics obtained with the 8 independent mocks extracted from the MDPL2 simulation (see [section 3.3](#)) as red triangles with error bars. The underlying cosmology of the simulation, shown by the black line, is well recovered by the estimator $\psi_1(r)$. Results ob-

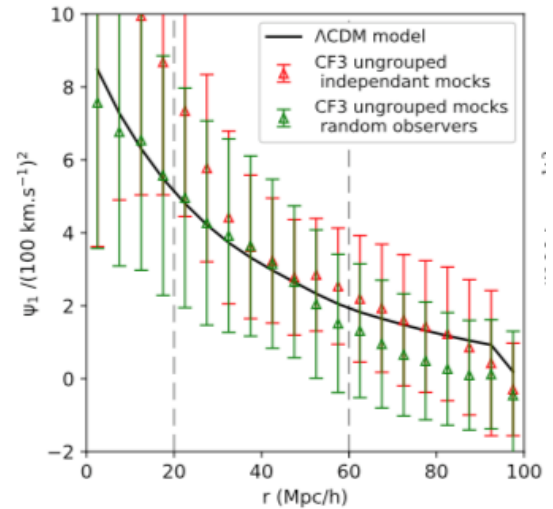


Figure 4. Peculiar velocity statistic ψ_1 as a function of the pair separation r computed in the large MDPL2 simulation box. The simulation's underlying Λ CDM model is shown as a black solid line. Red scattered triangles with error bars represent results obtained from the 8 CF3-like independent mocks. Green scattered triangles with error bars represent results obtained from the 100 CF3-like mocks constructed with randomly positioned observers. Vertical dashed lines show the region where $f\sigma_8$ can be fitted, see the limitations described in the text.

tained with the 100 CF3-like mocks generated considering random observers in the MDPL simulation is shown in [Figure 4](#) as green triangles with error bars. The underlying cosmology of the simulation is once again well recovered. This shows that despite its depth, the CF3 catalog may allow measuring the growth rate of large scale structures. Nevertheless, errors bars due to cosmic variance and the extent of

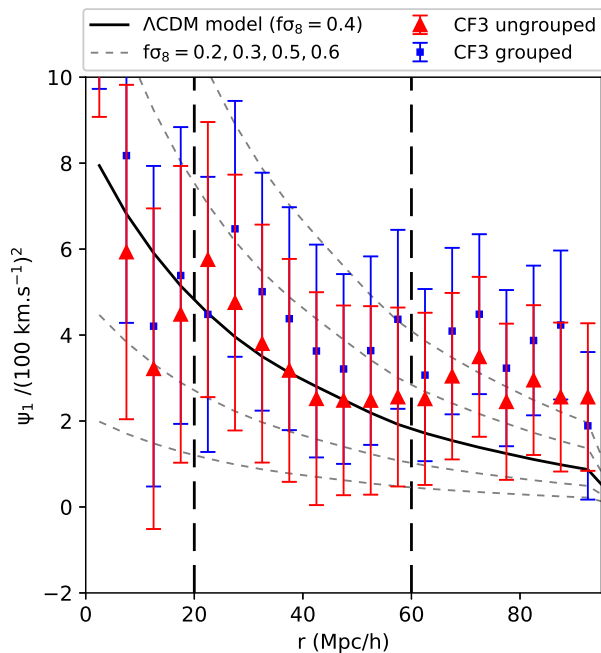


Figure 5. Observed peculiar velocity statistic ψ_1 as a function of the pair separation r . The Λ CDM model, $f\sigma_8 = 0.4$, predicted for CF3 galaxies is shown as a black solid line. Peculiar velocity statistics predicted for other cosmological models, $f\sigma_8 = 0.2, 0.3, 0.5, 0.6$, are shown as black dashed and dotted lines. Scattered points with error bars represent results obtained from observed peculiar velocities. The ungrouped sample of CF3 is shown as red triangles and the grouped CF3 sample is shown as blue squares. Vertical dashed lines show the region where $f\sigma_8$ can be fitted, see the limitations described in the text.

the sample are large and cannot be ignored. They must be taken into account when constraining $f\sigma_8$ with CF3 data.

4.2 Estimation of $f\sigma_8$ on data

Figure 5 shows the results of the computation of ψ_1 on the CF3 observations, for the ungrouped and grouped samples represented respectively as red triangles and blue squares. Errors bars include both, observational and cosmic variance uncertainties. Predictions of statistic ψ_1 for different cosmological models are shown as solid (Λ CDM, $f\sigma_8 = 0.4$) and dotted ($f\sigma_8 = 0.2, 0.3, 0.5, 0.6$) lines. The two estimators obtained for CF3 peculiar velocities are consistent with Λ CDM within their interval of robustness, as predicted by tests on mocks shown in Figure 3. Besides, one can observe that results obtained from CF3 groups have a slightly larger amplitude than results derived from CF3 galaxies.

For completeness, ψ_1 has also been applied to the previous CF2 catalog (not shown). The results are similar to CF3 and also in agreement with Λ CDM.

The data in Figure 5 are fitted by minimizing the χ^2 defined in equation 17. The fits are done within the interval [20, 60] $\text{Mpc } h^{-1}$ of pair separation distances. The results are displayed in Table 1 which shows the values of $f\sigma_8$ fitted directly from observational data. Both observational and

Table 1. Constraints of the normalized growth rate $f\sigma_8$ obtained from measurements of the peculiar velocity statistic ψ_1 , within its interval of robustness as described in the text, on the *Cosmicflows* datasets of observed peculiar velocities. The two last columns $\Delta f\sigma_8^{\text{obs}}$ and $\Delta f\sigma_8^{\text{cosmic}}$ correspond to observational and cosmic variance uncertainties on the constrained parameter respectively.

CF3 sample — statistic	$f\sigma_8$	$\Delta f\sigma_8^{\text{obs}}$	$\Delta f\sigma_8^{\text{cosmic}}$
CF3 ungrouped	0.43 ± 0.03	± 0.03	± 0.11
CF3 grouped	0.45 ± 0.04	± 0.04	± 0.11

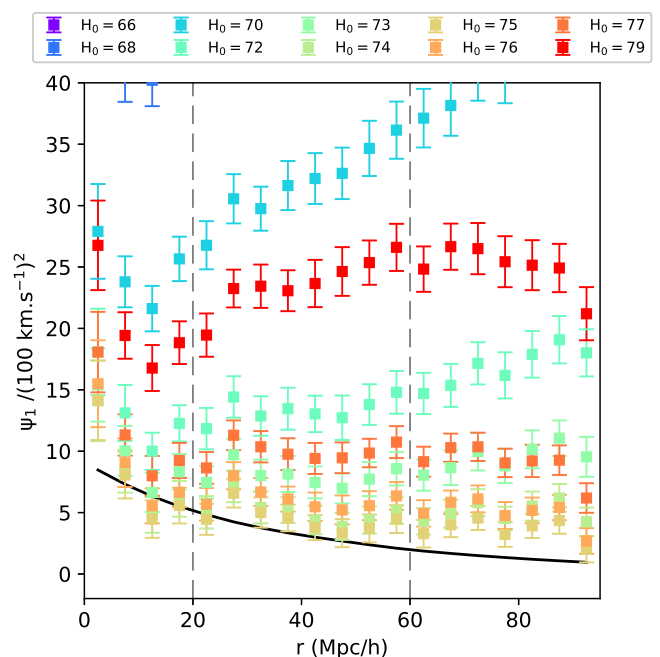


Figure 6. Observed peculiar velocity statistic ψ_1 as a function of the pair separation r . The Λ CDM model, $f\sigma_8 = 0.4$, predicted for CF3 galaxies is shown as a black solid line. Scattered points with error bars represent results obtained from observed peculiar velocities of the CF3 galaxies, derived by considering different values of the Hubble constant $H_0 = [66, 68, 70, 72, 73, 74, 75, 76, 77, 79]$ km/s/Mpc.

cosmic variance uncertainties on the constrained growth rate are reported.

Results shown in Figure 5 and Table 1 are obtained using the radial peculiar velocities computed from CF3 distances with equation 1 and $H_0 = 75 \text{ km s}^{-1} \text{ Mpc}^{-1}$. However, Tully et al. (2016) suggested that the range $H_0 = 75 \pm 2 \text{ km s}^{-1} \text{ Mpc}^{-1}$ gives a reasonable value for the monopole flow. This uncertainty on the Hubble constant may affect the uncertainty on the growth rate measurements, as the amplitude of ψ_1 depends on the chosen value of H_0 when deriving radial peculiar velocities, as shown in Figure 6. Therefore, we considered other values of H_0 within the error range given in Tully et al. (2016). Taking $H_0 = 73 \text{ km s}^{-1} \text{ Mpc}^{-1}$ to com-

pute peculiar velocity of CF3 galaxies gives $f\sigma_8 = 0.58 \pm 0.03$, and taking $H_0 = 77 \text{ km s}^{-1} \text{ Mpc}^{-1}$ gives $f\sigma_8 = 0.54 \pm 0.03$.

Wang et al. (2018) show a similar study in the Fig7 of their paper. They published error bars that are twice smaller than the ones we derived for ψ_1 (see Fig8 of Wang et al. (2018)).

Figure 7 shows the normalized growth rate $f\sigma_8$ as a function of redshift z . The black solid line corresponds to the Λ CDM model ($\gamma = 0.55$). Other cosmological models (modified gravity, $\gamma \neq 0.55$) are represented by dotted and dashed black lines. Scattered points with error bars show results taken from literature summarized in Table 2. Colors depend on the cosmological probe used to constraint the growth rate: SN Ia in yellow (Turnbull et al. 2012), galaxy peculiar velocities in blue (Johnson et al. 2014), Baryon Acoustic Oscillations in green (Blake et al. 2011; Reid et al. 2012) and Redshift Space Distortions in pink (Hawkins et al. 2003; Samushia et al. 2012; Beutler et al. 2012; de la Torre et al. 2013). Growth rate measurements predictions for future cosmological surveys are shown in red, with a predicted error bar of 10 per cent (McConnachie et al. 2016; Amendola et al. 2016; da Cunha et al. 2017).

Local growth rate constraint obtained from radial peculiar velocities of CF3 galaxies is shown in Figure 7 as a blue point with error bars. Errors bars include the observational uncertainties only, in coherence with other data points.

5 CONCLUSION

This article presents a measurement of the local value of $f\sigma_8$ in the nearby universe by means of a peculiar velocity survey: *Cosmicflows-3*. We obtained a measurement of $f\sigma_8 = 0.43 (\pm 0.03)_{\text{obs}} (\pm 0.11)_{\text{cosmic}}$ out to $z = 0.05$. Uncertainties correspond to observational "obs" and cosmic variance "cosmic" uncertainties respectively. This is in complete agreement with the measurement made by Wang et al. (2018), finding $f\sigma_8 = 0.488$.

Currently, as seen in Figure 7 some local cosmological probes like BAO and RSD do not have error bars that could constrain the growth rate of large scale structures. Even large redshift surveys such as SDSS, VIPERS or WiggleZ have a too large observational error budget to discriminate a cosmological model. In contrast, one can see that using only a few thousands of peculiar velocities of galaxies as cosmological probes to measure $f\sigma_8$ allows to restrict the range of cosmological models. However, due to the unique geometry of the CF3 survey as well as its sparseness, we have found that we are unable to use the full arsenal of velocity field statistics to probe $f\sigma_8$. We look forward to increased coverage to improve on this situation.

Upcoming redshift and peculiar velocity surveys (such as TAIPAN, MeerKAT, WALLABY, Euclid and MSE) are expected to improve uncertainties in a large range of redshifts from the very local universe up to $z = 1.7$. Hopefully this will allow to constrain the results also in cosmic variance allowing finally to discriminate a single cosmological model using galaxy 2-point statistics of peculiar velocities.

ACKNOWLEDGMENTS

Noam Libeskind, Carlo Schimd, Romain Graziani, Yannick Copin and Mickael Rigault are gratefully thanked for scientific discussions. Support has been provided by the Institut Universitaire de France and the CNES.

The CosmoSim database used in this article is a service by the Leibniz-Institute for Astrophysics Potsdam (AIP). The MultiDark database was developed in cooperation with the Spanish MultiDark Consolider Project CSD2009-00064.

REFERENCES

- Adams C., Blake C., 2017, *MNRAS*, **471**, 839
 Amendola L., et al., 2016, preprint, ([arXiv:1606.00180](https://arxiv.org/abs/1606.00180))
 Beutler F., et al., 2012, *MNRAS*, **423**, 3430
 Blake C., et al., 2011, *MNRAS*, **418**, 1707
 Born M., Green H. S., 1946, *Proceedings of the Royal Society of London Series A*, **188**, 10
 Carrick J., Turnbull S. J., Lavaux G., Hudson M. J., 2015, *MNRAS*, **450**, 317
 Davis M., Peebles P. J. E., 1977, *ApJS*, **34**, 425
 Djorgovski S., Davis M., 1987, *ApJ*, **313**, 59
 Dressler A., 1987, *ApJ*, **317**, 1
 Feldman H., et al., 2003, *ApJ*, **596**, L131
 Ferreira P. G., Juszkiewicz R., Feldman H. A., Davis M., Jaffe A. H., 1999, *ApJ*, **515**, L1
 Giovanelli R., Haynes M. P., Salzer J. J., Wegner G., da Costa L. N., Freudling W., 1994, *AJ*, **107**, 2036
 Giovanelli R., Haynes M. P., Herter T., Vogt N. P., Wegner G., Salzer J. J., da Costa L. N., Freudling W., 1997a, *AJ*, **113**, 22
 Giovanelli R., Haynes M. P., Herter T., Vogt N. P., da Costa L. N., Freudling W., Salzer J. J., Wegner G., 1997b, *AJ*, **113**, 53
 Gorski K., 1988, *ApJ*, **332**, L7
 Gorski K. M., Davis M., Strauss M. A., White S. D. M., Yahil A., 1989, *ApJ*, **344**, 1
 Hall A., 2018, arXiv e-prints, p. [arXiv:1811.05454](https://arxiv.org/abs/1811.05454)
 Hawkins E., et al., 2003, *MNRAS*, **346**, 78
 Haynes M. P., Giovanelli R., Salzer J. J., Wegner G., Freudling W., da Costa L. N., Herter T., Vogt N. P., 1999a, *AJ*, **117**, 1668
 Haynes M. P., Giovanelli R., Chamaraux P., da Costa L. N., Freudling W., Salzer J. J., Wegner G., 1999b, *AJ*, **117**, 2039
 Hellwing W. A., Nusser A., Feix M., Bilicki M., 2016, preprint, ([arXiv:1609.07120](https://arxiv.org/abs/1609.07120))
 Hoffman Y., Ribak E., 1991, *ApJ*, **380**, L5
 Hudson M. J., 1994, *MNRAS*, **266**, 475
 Hudson M. J., Turnbull S. J., 2012, *ApJ*, **751**, L30
 Huterer D., Shafer D., Scolnic D., Schmidt F., 2016, preprint, ([arXiv:1611.09862](https://arxiv.org/abs/1611.09862))
 James F., Roos M., 1975, *Computer Physics Communications*, **10**, 343
 Johnson A., et al., 2014, *MNRAS*, **444**, 3926
 Jones D. H., et al., 2004, *MNRAS*, **355**, 747
 Jones D. H., Peterson B. A., Colless M., Saunders W., 2006, *MNRAS*, **369**, 25
 Jones D. H., et al., 2009, *MNRAS*, **399**, 683
 Juszkiewicz R., Fisher K. B., Szapudi I., 1998, *ApJ*, **504**, L1
 Juszkiewicz R., Springel V., Durrer R., 1999, *ApJ*, **518**, L25
 Juszkiewicz R., Ferreira P. G., Feldman H. A., Jaffe A. H., Davis M., 2000, *Science*, **287**, 109
 Kaiser N., 1990, *Contemporary Physics*, **31**, 149
 Karachentsev I. D., Karachentseva V. E., Kudrya Y. N., Makarov D. I., Parnovsky S. L., 2000, *Bulletin of the Special Astrophysics Observatory*, **50**, 5

Table 2. Measurements of normalized growth rate $f\sigma_8$ at redshift z taken from literature. These constraints are obtained by using various cosmological probes: peculiar velocities (Vpec), Type Ia Supernovae (SN Ia), Redshift Space Distortions (RSD) and Baryon Acoustic Oscillations (BAO).

	Redshift z	Normalized growth rate $f\sigma_8$	Publication	Cosmological probe
6dFGS	0.05	$0.428^{+0.079}_{-0.068}$	Johnson et al. (2014)	Vpec
A1	0.03	0.40 ± 0.07	Turnbull et al. (2012)	SN Ia
2dFGRS	0.20	0.46 ± 0.07	Hawkins et al. (2003)	RSD
6dFGRS	0.067	0.423 ± 0.055	Beutler et al. (2012)	RSD
WiggleZ	0.22	0.42 ± 0.07	Blake et al. (2011)	BAO
	0.41	0.45 ± 0.04		
	0.60	0.43 ± 0.04		
	0.78	0.38 ± 0.04		
SDSS-LRG	0.25	0.3512 ± 0.0583	Samushia et al. (2012)	RSD
	0.37	0.4602 ± 0.0378		
BOSS	0.57	0.451 ± 0.025	Reid et al. (2012)	BAO
VIPERS	0.80	0.47 ± 0.08	de la Torre et al. (2013)	RSD

- Kirkwood J. G., 1946, *J. Chem. Phys.*, **14**, 180
Kirkwood J. G., 1947, *J. Chem. Phys.*, **15**, 72
Lahav O., Lilje P. B., Primack J. R., Rees M. J., 1991, *MNRAS*, **251**, 128
Lavaux G., Hudson M. J., 2011, *MNRAS*, **416**, 2840
Ma Y.-Z., Li M., He P., 2015, *A&A*, **583**, A52
McConnachie A., et al., 2016, preprint, ([arXiv:1606.00043](https://arxiv.org/abs/1606.00043))
Monin A. S., Yaglom A. M., 1975, *Statistical fluid mechanics*. Cambridge: MIT Press
N. N. Bogoliubov 1946, *Journal of Experimental and Theoretical Physics*, **16**, 691
Nusser A., 2017, *MNRAS*, **470**, 445
Peebles P. J. E., 1976, *ApJ*, **205**, 318
Peebles P. J. E., 1980, *The large-scale structure of the universe*
Peebles P. J. E., 1987, *Nature*, **327**, 210
Planck Collaboration et al., 2016, *A&A*, **594**, A13
Prada F., Klypin A. A., Cuesta A. J., Betancort-Rijo J. E., Primack J., 2012, *MNRAS*, **423**, 3018
Reid B. A., et al., 2012, *MNRAS*, **426**, 2719
Samushia L., Percival W. J., Raccanelli A., 2012, *MNRAS*, **420**, 2102
Saunders W., et al., 2000, *MNRAS*, **317**, 55
Strauss M. A., Willick J. A., 1995, *Phys. Rep.*, **261**, 271
Tully R. B., Fisher J. R., 1977, *A&A*, **54**, 661
Tully R. B., et al., 2013, *AJ*, **146**, 86
Tully R. B., Courtois H. M., Sorce J. G., 2016, *AJ*, **152**, 50
Turnbull S. J., Hudson M. J., Feldman H. A., Hicken M., Kirshner R. P., Watkins R., 2012, *MNRAS*, **420**, 447
Wang Y., Rooney C., Feldman H. A., Watkins R., 2018, preprint, ([arXiv:1808.07543](https://arxiv.org/abs/1808.07543))
Watkins R., Feldman H. A., 2015, *MNRAS*, **450**, 1868
Willick J. A., Courteau S., Faber S. M., Burstein D., Dekel A., 1995, *ApJ*, **446**, 12
Willick J. A., Courteau S., Faber S. M., Burstein D., Dekel A., Kolatt T., 1996, *ApJ*, **457**, 460
Willick J. A., Courteau S., Faber S. M., Burstein D., Dekel A., Strauss M. A., 1997, *ApJS*, **109**, 333
Yasini S., Mirzhatuny N., Pierpaoli E., 2018, arXiv e-prints, p. [arXiv:1812.04241](https://arxiv.org/abs/1812.04241)
Yvon J., 1935, *La théorie statistique des fluides et l'équation d'état*. Actualités scientifiques et industrielles, Hermann & cie, https://books.google.fr/books?id=5LI_AQAIAAJ
Zaroubi S., Hoffman Y., Fisher K. B., Lahav O., 1995, *ApJ*, **449**, 446
Zaroubi S., Hoffman Y., Dekel A., 1999, *ApJ*, **520**, 413
da Costa L. N., Bernardi M., Alonso M. V., Wegner G., Willmer C. N. A., Pellegrini P. S., Rit e C., Maia M. A. G., 2000, *AJ*, **120**, 95
da Cunha E., et al., 2017, *Publ. Astron. Soc. Australia*, **34**, e047
de la Torre S., et al., 2013, *A&A*, **557**, A54

This paper has been typeset from a $\text{\TeX}/\text{\LaTeX}$ file prepared by the author.

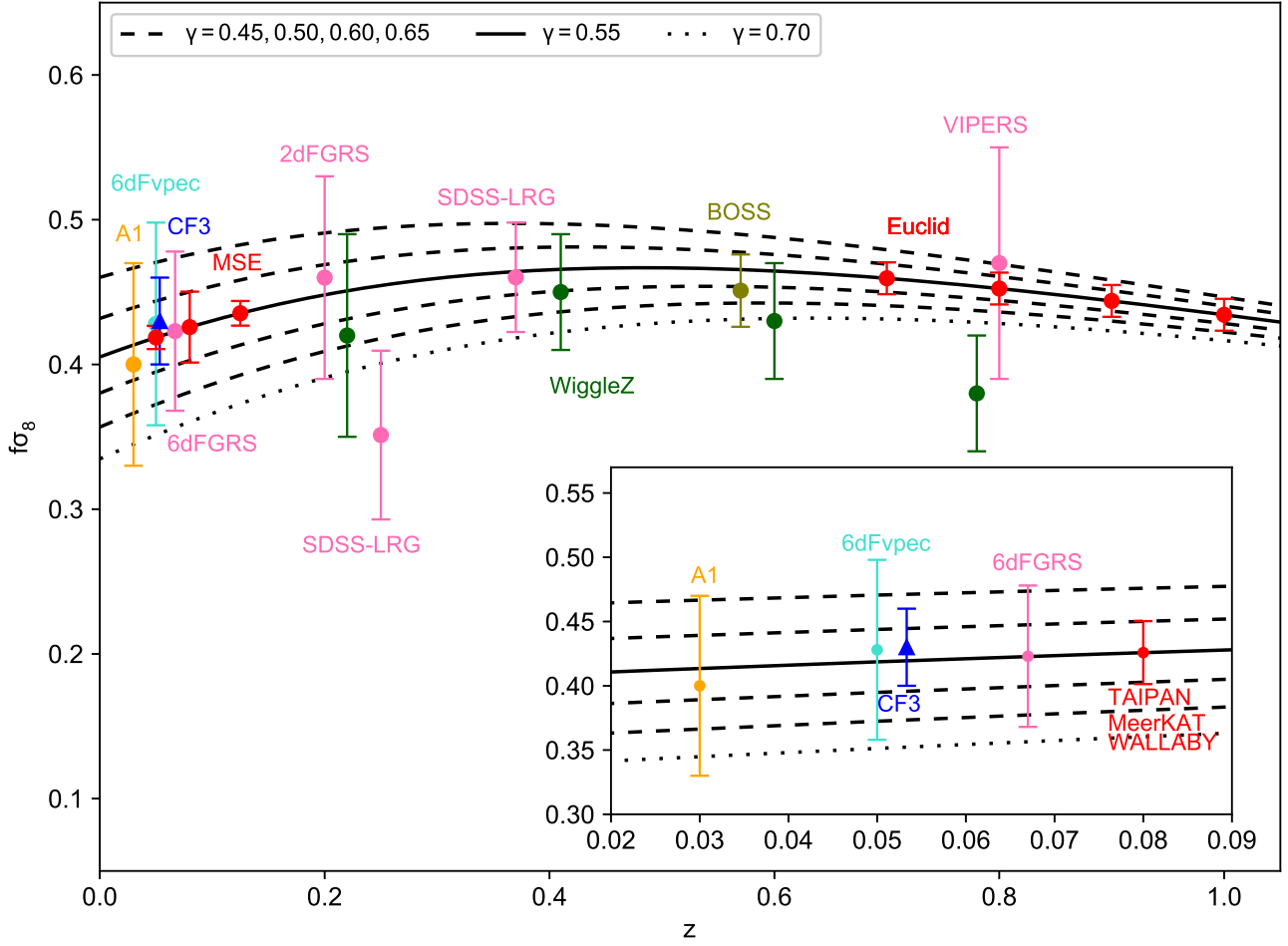


Figure 7. Normalized growth rate $f\sigma_8$ as a function of the redshift z . The Λ CDM model ($\gamma = 0.55$) is represented by a black solid line. Dotted and dashed black lines correspond to other cosmological models. Results taken from literature and displayed in Table 2 are shown by scattered points with error bars. Colors depend on the cosmological probe used to constraint the growth rate: SN Ia in yellow, galaxy peculiar velocities in light blue, Baryon Acoustic Oscillations in green and Redshift Space Distortions in pink. Growth rate measurements predictions for future cosmological surveys are shown in red. Result of this article obtained from observed peculiar velocities of CF3 galaxies is represented by a blue point with error bars. Errors bars include observational uncertainties only.